Figures of merit of avalanche-mode silicon LEDs

R. J. E. Hueting, S. Dutta, V. Agarwal, A. J. Annema

R. J. E. Hueting, S. Dutta, V. Agarwal, A. J. Annema, "Figures of merit of avalanche-mode silicon LEDs," Proc. SPIE 11043, Fifth Conference on Sensors, MEMS, and Electro-Optic Systems, 1104305 (24 January 2019); doi: 10.1117/12.2501315

SPIE.

Event: Fifth Conference on Sensors, MEMS, and Electro-Optic Systems, 2018, Skukuza, South Africa

Figures of merit of avalanche-mode silicon LEDs

R.J.E. Hueting[1], S. Dutta[2], V. Agarwal[3], and A.J. Annema[1]

[1]MESA+ Institute for Nanotechnology, University of Twente, Enschede, The Netherlands
[2]Presently with LioniX International, Enschede, The Netherlands
[3]Presently with ItoM, Enschede, The Netherlands

ABSTRACT

The silicon avalanche-mode light-emitting diode (AMLED) opens a route for on-chip opto-electronic applications in standard CMOS, both due to its relatively broad spectral overlap with the spectral responsivity of silicon photodiodes and due to its high speed capability. This work presents closed form models for the key figures of merit (FOMs) of AMLEDs, namely, current (or power) density, cut-off frequency, radiative efficiency, and specifically for optical data communication energy cost per photon. Their derivations are based on one-dimensional analyses of an abrupt single-sided (p^+n or n^+p) junction and of a p-i-n diode. TCAD simulations for optimized device structures, including the recently reported superjunction (SJ) LED, were performed to validate the model. Measurements on single-sided abrupt junctions and SJ diodes are shown to validate some of the modelled trends. The results show that a p-i-n or an SJ diode is favorable to a conventional single-sided junction diode for the AMLED design. In addition, as confirmed for conventional AMLEDs by earlier reports, the results indicate that for a yet higher efficiency the carrier supply should be increased. For this a combination of a separate minority carrier injector and SJLED is proposed, referred to as the injection-avalanche CMOS SJLED. However, more experimental optical data (*e.g.*, absolute photon flux) are needed for a more accurate model validation.

Keywords: avalanche, CMOS, figures of merit, light-emitting diode, p-i-n diode, silicon, superjunction

1. INTRODUCTION

Light emission from silicon (Si) p-n junctions operating in avalanche breakdown [1], [2] is caused by a high electric field yielding high energy transitions of electrons to the valence band [3]. Consequently, these junctions exhibit broad-spectrum electro-luminescence (EL) at short wavelengths (λ∼350-900 nm), that have a significant overlap with the spectral responsivity of Si photo-diodes [4], although at a low power efficiency. Avalanche-mode operation is also beneficial from viewpoint of speed [5]. Combined, avalanche-mode light-emitting diodes (AMLEDs) open an alternative route towards intra-chip optical data communication [4], [6]-[11]. However for this several hurdles should be taken for optimal performance [12]. The first one is that the relatively high power consumption of the AMLED should be minimized. Second, the speed of the whole system could become an issue, and third, the data transfer should be with a minimal bit error rate (BER) along with a minimal required energy per photon (ζ). For both the BER and ζ, among other things, the optical efficiency (η_{RAD}) of AMLEDs should be increased as discussed further in this work. Ways to increase η_{RAD} of AMLEDs have been reported [7], [13], for which a physical model, to connect with device parameters, can add further understanding. Moreover, a small-signal modulation speed of AMLEDs of up to ~20 GHz has been experimentally investigated [5], which motivated us to investigate the underlying principle. In addition, for determining the power consumption a closed form model for the avalanche current is needed that in turn could be used for other figures of merit (FOMs).

Therefore in this work, closed form physics-based models for the key FOMs of AMLEDs, namely, the avalanche current density (J), cut-off frequency (f_{T}), η_{RAD} and ζ have been derived based on one-dimensional (1-D) analyses using a deterministic local multiplication model [14]. Traditional deterministic local avalanche models (*e.g.*, [15]) of the avalanche current density J rely on the multiplication factor where the injection or leakage current contribution of only one carrier (*i.e.*, J_{n0} for electrons or J_{p0} for holes) is included. By including both J_{n0} and J_{p0}, a more accurate J-V slope near breakdown

Fifth Conference on Sensors, MEMS, and Electro-Optic Systems, edited by Monuko du Plessis,
Proc. of SPIE Vol. 11043, 1104305 · © 2019 SPIE · CCC code: 0277-786X/19/$18 · doi: 10.1117/12.2501315

can be obtained [14]. However, for Si our model is applicable for a breakdown voltage $V_{BR} \gtrsim 5$ V. As reported earlier [16], because of non-local avalanche the effective field, and therefore the EL, of the Si single-sided junction diode will drop for $V_{BR} < 5$ V, as was experimentally confirmed in a 65nm bulk CMOS technology [17]. Even so, band-to-band tunneling [17] could then also play a role which makes the use of Si LED below 5V breakdown less attractive anyway. Therefore our model in [14] is here extended for the key FOMs in both p-i-n and single-sided abrupt diodes. Model validation is done using TCAD simulations (Sentaurus, version H-2013.03) for optimized device structures: an abrupt n^+p junction, a p-i-n diode, and the recently proposed p-n superjunction (SJ) LED ([18], see Fig. 1). Further, measured steady-state *I-V* characteristics and some optical measurements are also compared.

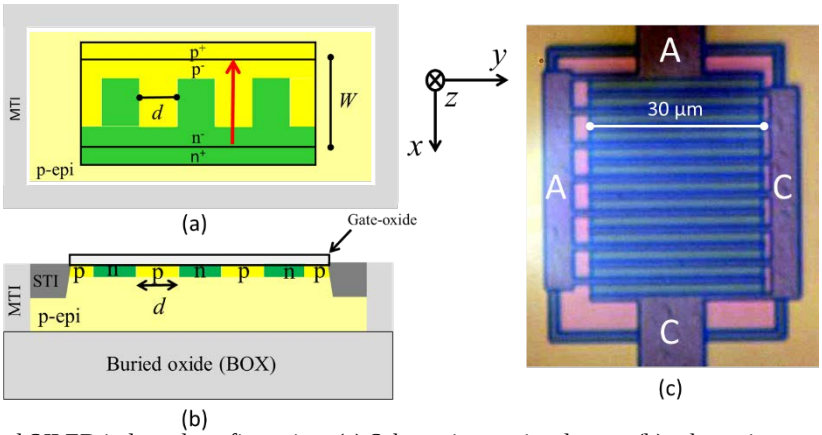

Figure 1: The proposed SJLED in lateral configuration: (a) Schematic top view layout, (b) schematic cross-section, and (c) a microphotograph of a realized SJLED [18] in an SOI CMOS technology [21]. The red arrow indicates the current flow direction.

2. DERIVATION OF FIGURES OF MERIT

In avalanche-mode (AM) the EL is governed by impact ionization and therefore by the reverse electric field *F* [16]. To increase η_{RAD}, power efficiency and speed of the LED, the EL-intensity per unit area should be enhanced [19]. Earlier, enhanced AM-EL was demonstrated with reported intensities up to 200 nW·µm^{-2} by enhancing the carrier injection (or J_{n0}) using a second emitter [3], [20], and through carrier momentum and energy engineering [19]. Recently, a new type of AMLED was reported, *i.e.* the superjunction (SJ) LED [18], realized in a 140-nm silicon-on-insulator (SOI)-CMOS technology [21], see Fig. 1. The basic idea is based on the reduced surface-field (RESURF) concept [22], [23] which is

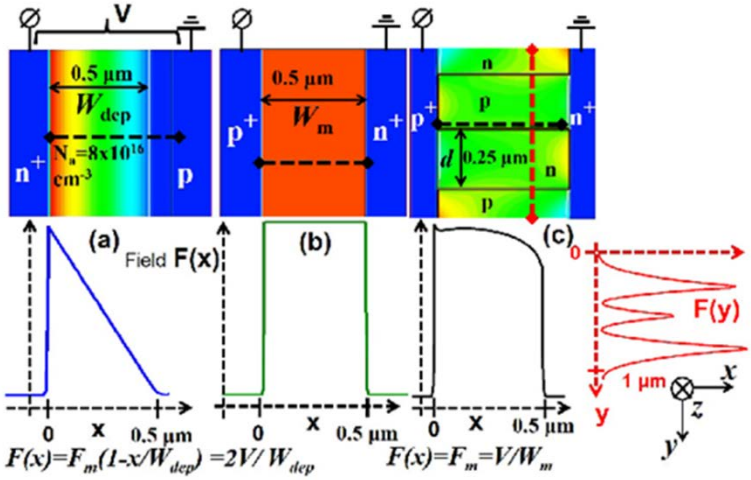

Figure 2 TCAD simulated electric field profiles (with 1-D cross-sections) in a (a) single-sided (n^+p) junction, (b) p-i-n diode, and (c) p-n SJ diode in this case with a pole-width of 0.25 µm (see Fig. 1 (c)). The SJ diode makes use of depleted alternate p- and n-type regions (repeated several times in the *y*-direction). For optimum RESURF [26], [30], a uniform field is formed in CMOS similar to that of a p-i-n diode. The integral of the electric field distribution represents V_{BR}, while the maximum field determines the light output [16]. As can be seen, for the same length of the active region *W* the p-i-n (and SJ) diode has (~$2^{2/3}$ times) higher V_{BR} compared to that of the n^+p diode.

especially widely adopted in power devices and smart power integrated circuits (ICs) [24]-[29]. The novelty of the SJLED is to mimic a p-i-n diode by obtaining a (more or less) constant field distribution at breakdown by the depletion width expansion ("JFET effect") of multiple alternately placed pn-junctions, which in turn improves the η_{RAD}. For better understanding why p-i-n diodes, and consequently SJLEDs, have a relatively high η_{RAD} we derive some closed form relations.

The 1-D electric field profiles $F(x)$ at reverse bias for an abrupt n^+p junction ($F(x) = F_{\mathrm{m}}(1 - x/W_{\mathrm{d}})$), and for a p-i-n diode ($F(x) = F_{\mathrm{m}}$) are shown in Fig. 2 (a) and (b), respectively. An optimized SJ diode [26] (Fig. 2(c)) is depicted that ensures a constant field distribution at reverse bias by alternately placing narrow p- and n- regions. In this way, depletion in the orthogonal dimension (y), *i.e.* optimum RESURF [26],[30], is achieved. Unlike focusing on the forward voltage (or on-resistance)-V_{BR} trade-off, as discussed in [26]-[30] for power devices, we focus on increasing the EL-V_{BR} dependence. The latter is achieved by obtaining a breakdown field (F_{C}) with uniform spatially, which can enhance avalanche-mode EL-intensity [16]. For our optical measurements, vertical structures with single-sided pn junctions (light received along the x-direction), and lateral structures for the SJ diode (light received along the z direction) are considered. However, for optocoupling such structures may be used in various orientations. Note that, there are some additional requirements for the SJ diode compared to a conventional p(-i-)n diode, as discussed in the appendix.

Under high reverse bias impact ionization becomes important, which is characterized by the ionization coefficients α_n and α_p, both being exponential functions of F [31]. When the maximum electric field $F_{\mathrm{m}} \geq F_{\mathrm{C}}$, the junction is in avalanche breakdown characterized by a manifold increase in current density J.

For obtaining closed form physics-based relations, Fulop's model [31] is used typically considering $\alpha_n = \alpha_p = \alpha$, to the avalanche breakdown condition [15]:

$$\int_0^W \alpha(x)dx = \int_0^W \alpha_{\mathrm{F}} F^7(x)dx = 1, \tag{1}$$

where $\alpha_{\mathrm{F}} = 1.8 \cdot 10^{-35}$ cm^{6}V^{-7} for Si, the active or space-charge region width W equals the multiplication width W_{m} and depletion width W_{d} for the p-i-n and single-sided abrupt diode, respectively. W_{m} is independent of the bias voltage V, while W_{d} is a function of V [15]. Note that in this work terms such as active, space-charge and depletion region are considered to be the same and the terms are used interchangeably without any intentional ambiguity. Further, without less of generality at breakdown (optimized) fully depleted single-sided junctions are considered, hence W_{m} and W_{d} represent the maximum device size.

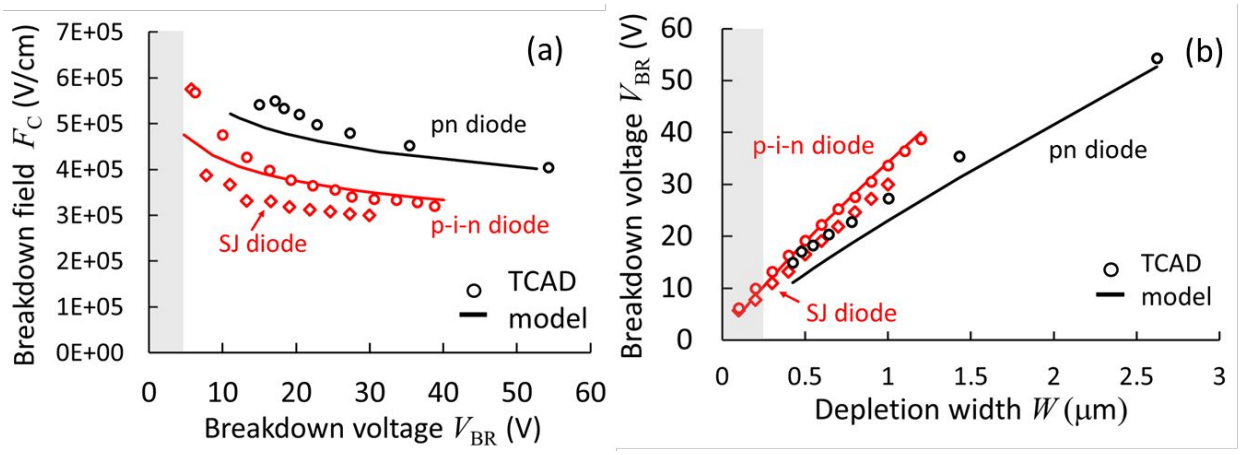

Figure 3 (a) Critical field F_{C} as a function of breakdown voltage V_{BR} (solid lines: model, open symbols: red diamonds represent SJ diode TCAD data, red open circles p-i-n diode TCAD data, and black open circles pn diode TCAD data). (b) V_{BR} against device width or depletion width W_{d} for the single-sided diode, and multiplication or active width W_{m} for the p-i-n diode. The grey zone indicates more or less where nonlocal avalanche effects play a role.

From Eq. (1), and the fact that $\int_0^W F(x)dx = V_{\mathrm{BR}}$, we obtain [16]:

$$F_{\mathrm{C,pin}} = (\alpha_{\mathrm{F}} \cdot V_{\mathrm{BR}})^{-1/6}, \tag{2a}$$

$$F_{\mathrm{C,n^+p}} = 2^{1/3}(\alpha_{\mathrm{F}} \cdot V_{\mathrm{BR}})^{-1/6}. \tag{2b}$$

Hence, at breakdown it can be stated that

$$W_{\mathrm{m}} = \alpha_{\mathrm{F}}^{1/6} \cdot V_{\mathrm{BR}}^{7/6}, \tag{3a}$$

$$W_{\mathrm{d}} = 2^{2/3} \cdot \alpha_{\mathrm{F}}^{1/6} \cdot V_{\mathrm{BR}}^{7/6} = 2^{2/3} \cdot W_{\mathrm{m}}. \tag{3b}$$

Fig. 3(a) shows F_{C} as a function of V_{BR} obtained from Eq. (2) and TCAD simulations. Minor differences are mainly because in Si $\alpha_n \neq \alpha_p$, as used in TCAD. F_{C} increases for lower V_{BR}, particularly for voltages less than about 10V. This is achieved by reducing W_{d} or W_{m} as shown in Fig. 3(b). Notably, for a p-i-n diode the same F_{C} is obtained for a lower V_{BR} (*i.e.*, less electrical power) compared to that for a single-sided diode. The TCAD extracted F_{C} for the SJ diode is slightly less than that for the p-i-n diode owing to a less uniform 2-D field distribution (see also Fig. 2 (b),(c)). Proper edge termination (*e.g.*, curved electrodes) is needed for uniform breakdown [30], which is outside the scope of this paper.

2.1 Avalanche current density (*J*)

Our model [14] is extended for both p-i-n and single-sided diodes, assuming $\alpha_n = \alpha_p = \alpha$. Focusing on electrons, we can derive:

$$J_n(x) = J_{n0} + \int_0^x \alpha(s) \cdot \left(J_{p0} + J_{n0} \cdot M_n(W)\right) ds, \tag{4a}$$

where the multiplication factor at the space-charge boundary ($x = W = W_{\mathrm{d}} \vee W_{\mathrm{m}}$) at a given bias $V \lesssim V_{\mathrm{BR}}$ is

$$M_n(W) = \frac{1 + \frac{J_{p0}}{J_{n0}} \int_0^W \alpha_{\mathrm{F}} \cdot F^7(x) dx}{1 - \int_0^W \alpha_{\mathrm{F}} \cdot F^7(x) dx}. \tag{4b}$$

Solving Eq. (4) we obtain for the p-i-n respectively single-sided diode:

$$J_{n,\mathrm{pin}}(x) = J_{n0} + \gamma \cdot \left(\frac{x}{W_{\mathrm{m}}}\right), \tag{5a}$$

$$J_{n,\mathrm{n^+p}}(x) = J_{n0} + \gamma \cdot \left(1 - \left(1 - \frac{x}{W_{\mathrm{d}}}\right)^8\right), \tag{5b}$$

with

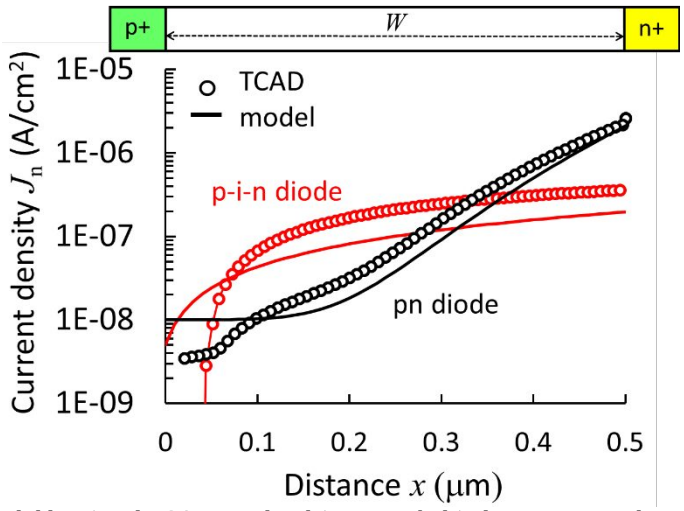

Figure 4 Modelled (solid lines) and TCAD simulated (open symbols) electron current density profile along the space-charge region in the n+p junction and p-i-n diode indicated above the graph, at a bias of $V_{\mathrm{R}} = V_{\mathrm{BR}} - 0.2$ V and $W_{\mathrm{d}} \approx W_{\mathrm{m}} = 0.5\mu$m. The coordinates are indicated in Fig. 1.

$$\gamma = \frac{\left(\frac{V_R}{V_{BR}}\right)^7}{\left(1-\left(\frac{V_R}{V_{BR}}\right)^7\right)}\left(J_{p0}+J_{n0}\right) = J\left(\frac{V_R}{V_{BR}}\right)^7 \qquad \wedge \qquad V_R \lesssim V_{BR}. \tag{6a}$$

For convenience sake the following parameter is introduced

$$\beta = \left(\frac{V_R}{V_{BR}}\right)^7 = 1 - \left(\frac{J_{p0}+J_{n0}}{J}\right), \tag{6b}$$

which is actually a measure for the ratio between the avalanche current and injection current ($(1-\beta)^{-1}$ equals the "I_{ON}/I_{OFF} ratio") of the AMLED.

In Fig. 4 the electron current density against the distance inside the space-charge region is shown for both the p-i-n and single-sided diode, where the model is compared with TCAD obtained results ($V_R = V_{BR} - 0.2$V). Good agreement has been obtained between the model and TCAD simulated $J_n(x)$ for both devices. Interestingly the results show for the p-i-n diode a linearly distributed current density, which implies that in this case the multiplication region more or less equals the depletion region (hence $W_m \approx W$).

Eqs. (5)-(6) hold for before and at the onset of breakdown, *i.e.* the multiplication factor goes to infinity. However once a high avalanche current is reached, *i.e.* $V_R \to V_{BR}$, the internal resistance of the diode becomes important. This resistance is mainly determined by the generated charge carriers in the depletion region. Focusing on electrons for the high injection current density holds then:

$$J_H = J_{nW} = -\frac{V_R-(V_{BR}-\delta V)}{\int_0^W \frac{1}{q\mu_n n}dx}, \tag{7}$$

where n is the electron concentration and μ_n is the electron mobility. The fit parameter $\delta V = V_{BR}\{1-(1-\beta)^{1/7}\} \ll 1$V is needed for numerical reasons. Since practically all electron charge have been formed at high field before any resistive effects played a role, it can be stated that $n = -\frac{J_n}{q v_{sat}}$ with v_{sat} is the saturation velocity ($v_{sat} \approx 10^7$ cm/s) [15].

After substituting Eq. (5a) in Eq. (7) it can be derived for the pin or SJ diode that

$$J_H = \frac{\mu_n \gamma_L \left(V_R-(V_{BR}-\delta V)\right)}{\alpha_F^{1/6} V_{BR}^{7/6} v_{sat} \ln\left(\frac{J_{n0}+\gamma_L}{J_{n0}}\right)}, \tag{8a}$$

and

$$\gamma_L = \frac{\left(\frac{(V_{BR}-\delta V)}{V_{BR}}\right)^7}{\left(1-\left(\frac{(V_{BR}-\delta V)}{V_{BR}}\right)^7\right)}\left(J_{p0}+J_{n0}\right), \tag{8b}$$

considering the generated charge carriers at $V_R = V_{BR} - \delta V$ induce the series resistance. For the single-sided diode the solution can only be obtained numerically, however in practice Eq. (8) could be used for this as well.

2.2 Cutoff frequency (f_T)

At avalanche breakdown, the current flow in a diode is dominated by (majority) carriers generated via impact ionization in the space-charge region. Moreover, drift of those carriers will play a role. The electrons flow to the n+ injector region and holes to the p+ injector region. Consequently, the small-signal modulation speed is largely determined by the transit time (τ_T) of the carriers across W_d and/or W_m. At or near breakdown the field is sufficiently high so that the carrier velocity reaches saturation [15].
Applying the quasi-static approach for electrons we get :

$$\tau_T = \left|\frac{\partial Q_n}{\partial J}\right| = q\int_0^W \frac{\partial n}{\partial J}dx \tag{9}$$

where q is the elementary charge ($q = 1.6 \cdot 10^{-19}$ C), Q_n is the integrated quasi-static electron charge (that equals the integrated quasi-static hole charge) at a given bias V_R across the device, and J is the total current density. The latter

equals the electron current density at the edge of the depletion layer, hence terminal, which in turn equals the hole current density at the other side of the depletion layer: $J = J_{nW} = J_{p0}$. The cutoff frequency can be calculated according to $f_T = 1/2\pi\tau_T$. The quasi-static approach is valid provided that $W < c/(n_{Si} f_T)$, where c is the speed of EM waves in free space ($c = 3 \cdot 10^8$ m/s) and n_{Si} being the silicon refractive index.

Again, at high field we have $n = -\frac{J_n}{q v_{sat}}$ [15]. By substituting this term in Eqs. (5) and (9) we obtain after some manipulation:

$$\tau_{T,pin} = \frac{1}{2}\frac{W_m}{v_{sat}}, \tag{10a}$$

and

$$\tau_{T,n^+p} = \frac{8}{9}\frac{W_d}{v_{sat}}, \tag{10b}$$

which implies that a p-i-n, and in principle an SJ, diode can be operated at about a ~3 higher speed for a given V_{BR}. Note that [5] reported a somewhat higher $\tau_{T,n^+p} = W_d/v_{sat}$.

An exercise was done for the TCAD simulated $n(x)$ and J by applying a perturbation of ΔV in the bias. Subsequently, the f_T was calculated. Good agreement between the model and TCAD (for both p-i-n and optimized SJ) has been obtained, see Fig. 5, except for some deviation at higher V_{BR} for the n^+p case. The latter is due to the non-uniformity of carrier drift velocity, caused by the lower F away from the junction ($x = 0$). Similar TCAD values for f_T were obtained deep in avalanche, indicating that the resistance of the space-charge region does not affect f_T.

There are two important remarks though. Firstly, in the analysis presented so far only the electrical response has been considered. However, at very high frequencies eventually the light emission will be forming the bottleneck rather than the charge storage. This strongly depends on the radiative lifetime (τ_{RAD}) which in turn is governed by the bimolecular radiative radiation coefficient ($\tau_{RAD} \propto 1/B_{RAD}$): once $\tau_T < \tau_{RAD}$ the f_T is no longer limited by charge storage rather by radiative recombination processes. If this was the case, Eq. (9) would not be applicable and then investigating the switching behavior could be an alternative way for determining B_{RAD}. Secondly, this section only discusses small-signal behavior as done in [5]. For more power efficient (and possibly robust) solutions it would be better to employ transient signals to the AMLED such that it is only turned on just at breakdown, and turned off below it [12],[32]. This is also referred to as On-Off Keying (OOK) [33],[34]. Although the small-signal analysis results in a measure for the ultimate speed, a more realistic OOK analysis is also needed and requires a separate study.

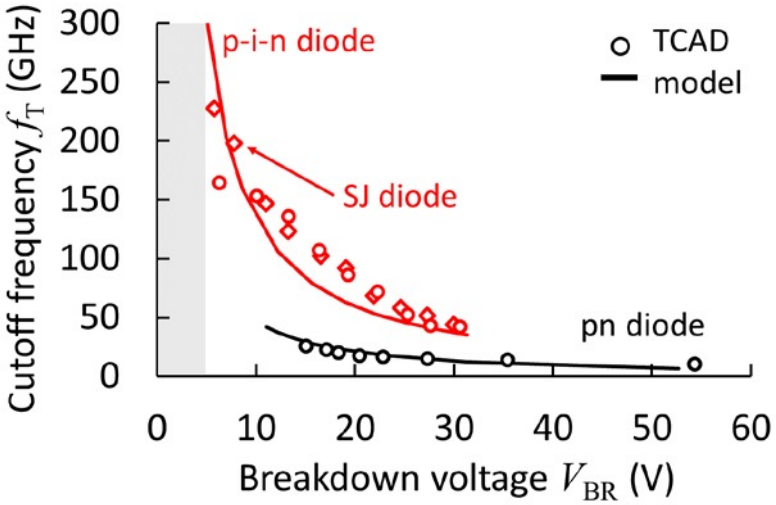

Figure 5 Modeled (solid lines) versus TCAD simulated (open symbols) f_T against V_{BR}. As W increases with increasing V_{BR}, the transit time (Eq. (10)) increases leading to a decrease in f_T. Further, both TCAD and our model yield a higher f_T for both the p-i-n diode (circles) and optimized SJ diode (diamonds) compared to the conventional counterpart. The grey zone indicates more or less where nonlocal avalanche effects play a role.

2.3 Radiative efficiency (η_{RAD})

For deriving a relation for the radiative efficiency we need first discuss what determines the radiative recombination rate. This is certainly not trivial for AMLEDs.

As reported earlier for conventional (forward biased) LEDs [35] for the radiative recombination rate holds that

$$R = B_{RAD} \cdot \left(p \cdot n - n_{\mathrm{i}}^2\right), \tag{11a}$$

with p is the hole concentration and

$$n_{\mathrm{i}}^2 = N_{\mathrm{C}} N_{\mathrm{V}} \cdot e^{\left(-\frac{E_{\mathrm{G}}}{kT}\right)}. \tag{11b}$$

N_{C}, N_{V} are the effective densities of states in the conduction respectively valence band, E_{G} is the bandgap, k is Boltzmann's constant ($k = 1.38 \cdot 10^{-23}$ J/K), and T is the ambient temperature.

There are some issues with Eq. (11) though related to AMLEDs. First, the *pn* product inside the active region is not constant. Second, for n_{i} we cannot use the bulk silicon value simply because the energy transitions are more direct and above E_{G}. The threshold energy needed for avalanche is $E_{\mathrm{TH}} \sim 3/2\, E_{\mathrm{G}}$ [36],[37], which is the *minimum* required energy for a transition. As a result, most probably we can assume that $n_{\mathrm{i}}^2 \lesssim e^{\left(-\frac{E_{\mathrm{TH}}}{kT}\right)} \approx 0$. Third, for Si in forward mode $B_{\mathrm{RAD}} \approx 10^{-14}$ cm^3 s^{-1} [38], [39], however this value could be higher for AM because there are field-assisted energy transitions with reduced momentum mismatch [19]. A possible complication is that B_{RAD} likely depends on F_{C}. For higher F_{C} values higher energy transitions are possible resulting in an increased absorption coefficient, that in turn determines B_{RAD} [39]. For simplicity sake we assume B_{RAD} to be a constant though, and we consider this parameter to be an "effective" B_{RAD}.

Therefore, the photon emission flux [16] R_{op} (cm^{-2}s^{-1}) can be obtained from the electron and hole concentration profiles (resp. $n(x)$ and $p(x)$) according to:

$$R_{\mathrm{op}} \approx B_{\mathrm{RAD}} \cdot \int_0^W p(x) n(x) dx = \frac{B_{\mathrm{RAD}}}{q^2 v_{\mathrm{sat}}^2} \int_0^W J_p(x) J_n(x) dx. \tag{12}$$

After some mathematical manipulation we obtain for the p-i-n diode

$$R_{\mathrm{op|pin}} \approx J^2 \frac{B_{\mathrm{RAD}} W_{\mathrm{m}}}{q\, v_{\mathrm{sat}}^2} \beta \left\{\frac{1}{2} - \frac{1}{3}\beta\right\}, \tag{13a}$$

and for the single-sided junction diode

$$R_{\mathrm{op|pn}} \approx J^2 \frac{B_{\mathrm{RAD}} W_{\mathrm{d}}}{q\, v_{\mathrm{sat}}^2} \beta \left\{\frac{8}{9} - \frac{128}{153}\beta\right\}, \tag{13b}$$

where the total current density $J = \gamma/\beta$, see Eq. (6).

The internal quantum (radiative) efficiency is defined as being the ratio of the flux of photons and that of the charge carriers:

$$\eta_{\mathrm{RAD}} \equiv \frac{\text{Flux photons}}{\text{Flux carriers}} = \frac{qR_{\mathrm{op}}}{J} \tag{14}$$

and can be obtained for the p-i-n diode by adopting Eqs. (13a), (14) and for the pn diode Eqs. (13b), (14). Importantly, in Eq. (13) the applied voltage is considered to be near the breakdown voltage, *i.e.* $\beta \to 1$ (in practice determined from the "$I_{\mathrm{ON}}/I_{\mathrm{OFF}}$ ratio"), hence $J \gg J_{n0} + J_{p0}$.

For the power efficiency it can be stated that [33]

$$\eta_{\mathrm{P}} \equiv \frac{P_{\mathrm{photons}}}{P_{\mathrm{electrical}}} = \frac{E_{\mathrm{photons}}}{E_{\mathrm{electrical}}} \approx \eta_{\mathrm{RAD}} \cdot \frac{1}{qV_{\mathrm{BR}}} \cdot \frac{hc}{\lambda}, \tag{15}$$

with h is Planck's constant ($6.6261 \cdot 10^{-34}$ J s) and λ is the wavelength (in our case ~650nm). E_{photons} and $E_{\mathrm{electrical}}$ is the photon energy respectively electric energy.

As can be seen from Eq. (15), compared to the internal quantum efficiency the power efficiency near breakdown ($V_{\mathrm{R}} \approx V_{\mathrm{BR}}$) shows the same dependencies with the current and recombination processes. The optical or EL intensity can be obtained by multiplying Eq. (13) with $hc/q\lambda$.

Finally, particularly for optocoupling we propose another figure of merit which is related to the above Eqs.:

$$\zeta = \frac{E_{\text{electrical}}}{\#\ \text{photons}} = \frac{P_{\text{electrical}}}{\text{Flux photons}} = \frac{qV_{\text{BR}}}{\eta_{\text{RAD}}}, \tag{16}$$

with $P_{\text{electrical}}$ is the areal electric power density. This FOM represents the energy cost per photon of the LED and obviously should be minimized. According to Eq. (16) this should be done by increasing η_{RAD} (for a not too high V_{BR}).

3. EXPERIMENTAL AND DISCUSSION

For validating our model, both quantitatively and qualitatively, there is some experimental evidence as well. A lateral stack of p-n junctions, each with a pole-width d (Fig. 1) was realized in a silicon-on-insulator (SOI) CMOS technology to construct an SJLED. This creates junction-folding and increases the areal density of high field regions resulting in a relatively high EL.

Fig. 6 shows the measured and TCAD simulated *I-V* characteristics for an SJ diode with d = 0.38 µm and a conventional (lateral) reference diode both with a same active length of W = 2µm [18]. As explained earlier, because of the constant field in the former V_{BR} has increased by a factor ~$2^{2/3}$ compared to the conventional diode. Moreover, the TCAD simulations are in line with the experiments. The leakage current of the conventional diode is higher than for the SJ counterpart, most probably because of the shallow trench isolation (STI) at the periphery directly contacting the junction in the former. This results in a reduction of the effective lifetime.

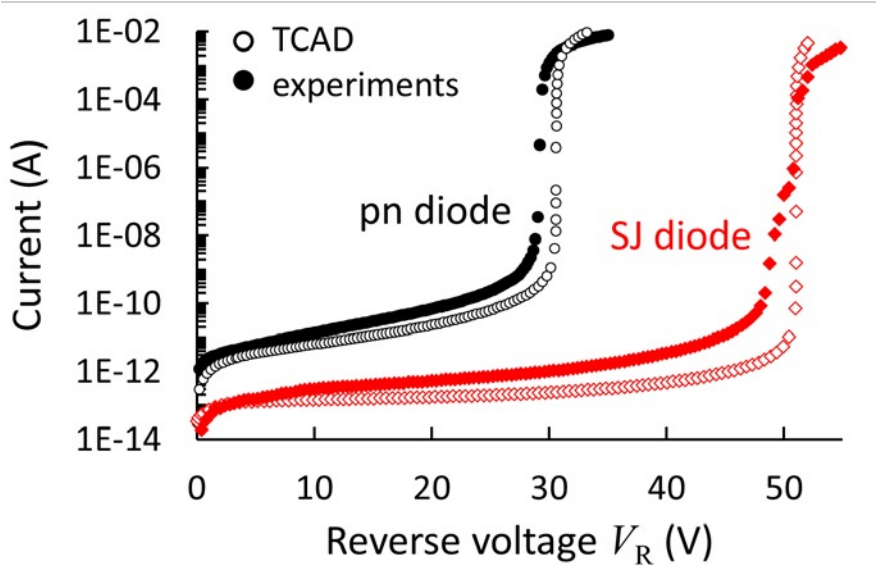

Figure 6 TCAD simulated and measured reverse I-V characteristics of a conventional lateral diode and an SJLED (d=0.38 µm, T=300K, A=780µm^2). The measurements were performed with a Keithley 4200SCS.

Fig. 7 shows a comparison of our SJLED model (Eqs. (5), (7)) with experimental/TCAD data for various SJ devices [18]. The model shows good agreement with the data where mainly two fit parameters are important: δV and J_{n0}. The breakdown voltage can be obtained from W (Eq. (3)). Further, Fig. 7(b) shows that for a smaller pole width, in this case improved RESURF (see appendix), the SJ diodes show a higher V_{BR} compared to the conventional counterpart.

The connection between the spatial uniformity in $F(x,y)$ and AM-electroluminescence (EL) is evident from Fig. 8, where AM-EL micrographs are shown for the (lateral) reference diode and three SJLEDs. For reference a top view microphotograph of such a realized SJLED is shown in Fig. 1 (c) from which EL was measured. In particular SJLEDs with a pole width d=0.38 µm show that RESURF leads to a more uniform light emission along the y-axis. The increase in the EL-area implies an increase in η_{RAD} [37] of the SJ-LED. It was estimated that for the optimum SJLED with d=0.38 µm $\eta_{\text{RAD}} = 2.67 \cdot 10^{-5}$. For d=0.58 µm $F(y)$ is less uniform than for d=0.38 µm. Under a given optical resolution, the non-

uniformity in the field distribution results in a discontinuous array of EL-spots for a large pole width. Each spot corresponds to a junction between p-type and n-type fingers.

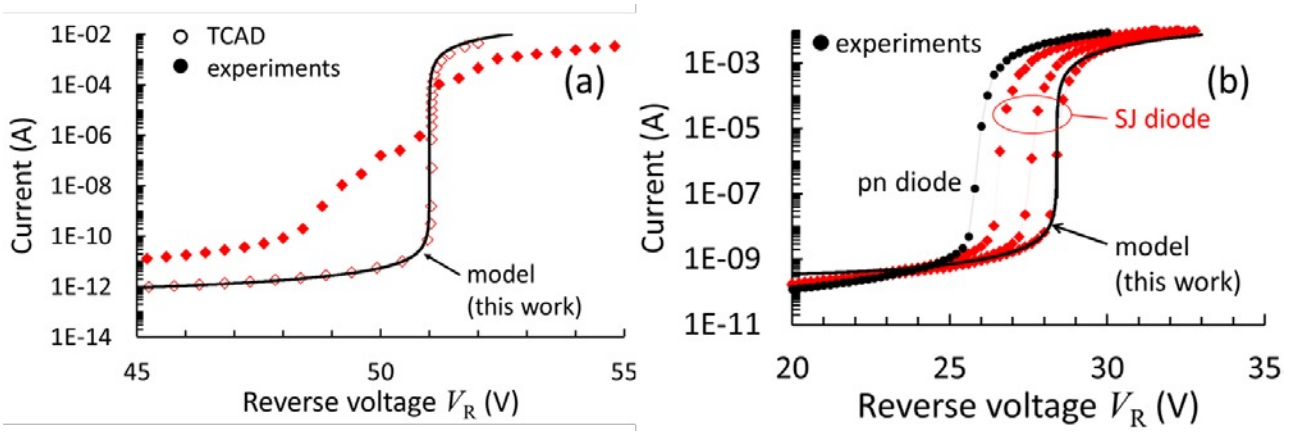

Figure 7 Comparison of our avalanche current model (drawn black lines, Eqs.(5), (7)) with experimental and TCAD data (closed resp. open symbols) obtained from various devices: (a) the SJLED presented in Fig. 6 ($W = 2\mu\text{m}, V_{\text{BR}} = 51\text{V}, J_{\text{n0}} \cdot A = 3.8 \cdot 10^{-13}A, \delta V = 10^{-11}\text{V}$, $\mu_n = 500\frac{\text{cm}^2}{\text{Vs}}, A = 780\ \mu\text{m}^2$), (b) a conventional LED and three SJLEDs with d varying from 0.38 (maximum breakdown voltage), 0.58 and 0.77μm ($W = 1\mu\text{m}, V_{\text{BR}} = 28.4\text{V}, J_{\text{n0}} \cdot A = 3.0 \cdot 10^{-10}A$, $\delta V = 5 \cdot 10^{-8}\text{V}$, $\mu_n = 500\ \text{cm}^2/\text{Vs}, A = 510\ \mu\text{m}^2$). The measurements were done with a Keithley 4200 SCS.

Fig. 9 shows a graphical output of the internal quantum efficiency, Eq. (13), and the energy per photon, Eq. (16), against V_{BR} for both the p-i-n diode and the single-sided diode. The results show higher efficiencies at the same V_{BR}, and consequently lower energies per photon, for the p-i-n diode compared to those of the single-sided diode. As explained before, this is due the constant field distribution of the former, where the depletion region equals the multiplication region, while for the single-sided diode mainly the (multiplication) region around the peak field is important. This yields more light emission spots, thereby an increased EL-intensity [16].

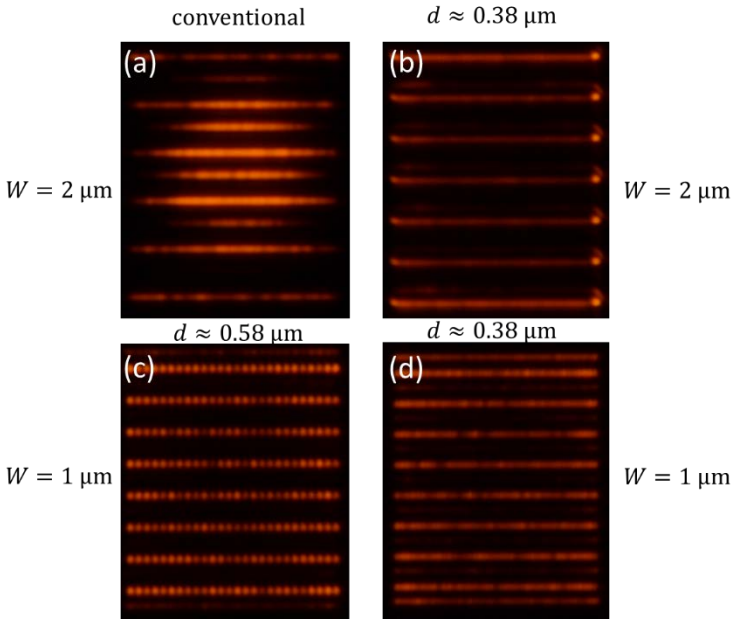

Figure 8 Avalanche mode EL micrographs obtained from realized LED structures presented in Fig. 1(c) (to the same scale), at a fixed current = 4 mA at 300 K with a visible-range camera and an integration time of 25 s: (a) a conventional AMLED, and SJLEDs with (b), (d) pole width d = 0.38μm, and with (c) d=0.58 μm. Light is received along the z-axis (vertically). Note that the metal lines on the electrodes screen the light.

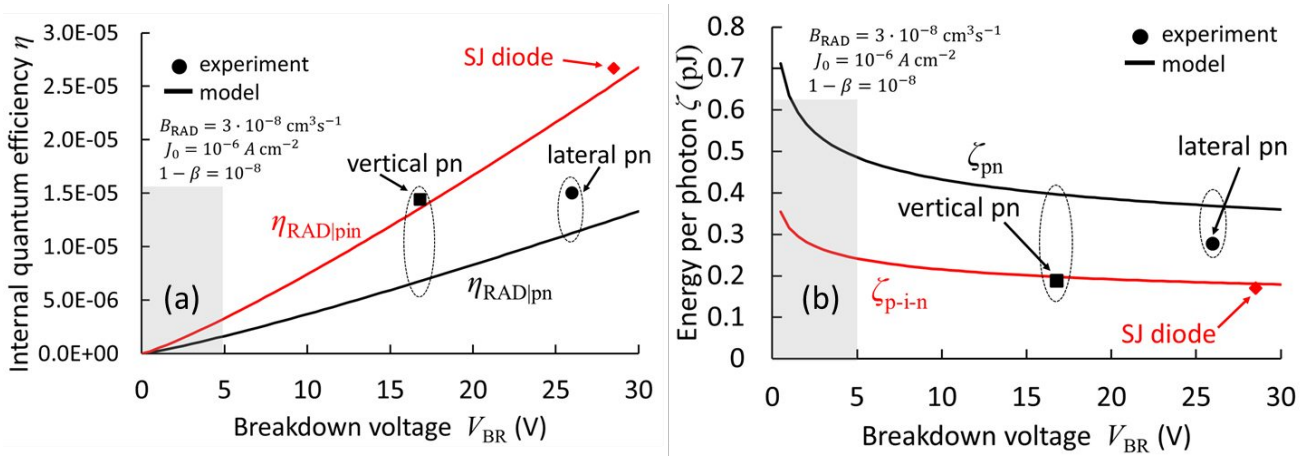

Figure 9 Calculated (a) internal quantum efficiencies and (b) required energy per photon for the p-i-n (Eqs. (13a), (14), (16)) resp. pn (Eqs. (13b)-(14), (16)) diode. The following parameters were used: $1-\beta = 10^{-8}, B_{RAD} = 3 \cdot 10^{-8}$ cm^{3}s^{-1}, $J_{n0} + J_{p0} = 10^{-6}$ A cm^{-2}. The symbols represent experimentally estimated values obtained from a vertical (black square) and lateral conventional (black circle) LED, and from an SJLED (d=0.38 µm, red diamond to be compared with the p-i-n diode model). The grey zone indicates more or less where nonlocal avalanche effects play a role.

Generally, for a higher V_{BR}, hence larger W, the $n(x)p(x)$ product increases, consequently R_{op} increases (see Eq. (12)). J also increases with V according to Eq. (5), but R_{op} increases at a faster rate, $\propto J^2$ (see Eq. (13)), leading to a net increase in η_{RAD}. In addition, there appears to be a tradeoff between the f_T and η_{RAD}, as reported for forward-bias mode Si LEDs [40]: the higher η_{RAD} (Fig. 9), the lower f_T (Fig. 5). This tradeoff is broken by adopting p-i-n diodes or SJLEDs. On the other hand care should be taken especially for $V_{BR} \lesssim 10$V because of the increase in F_C (see Fig. 3(a)) which could influence B_{RAD}. Fig. 9 shows good agreement with the experimentally estimated η_{RAD} values of a lateral (conventional) pn diode and the SJ diode (d=0.38 µm). For these estimations an on-chip Si photodiode was used. However our model does not include reabsorption, which implies that the extracted B_{RAD} may be different depending on the device architecture and (type of) measurement. As a result, there is a discrepancy between the model and the experimentally estimated η_{RAD} obtained from a vertical diode [41] (using an off-chip photodiode).

Further, for different LEDs the photon flux was measured as a function of the reverse voltage, see Fig. 10. Unfortunately our equipment was not suited for determining the absolute photon flux, rather we were able to measure a trend. Fig. 10 shows good agreement between the measured (for the vertical diode reported in [41] and a non-optimized SJ diode) and modeled trends for R_{op} against V. The inset of Fig. 10(b) shows the emission spectra of the particular SJ diode.

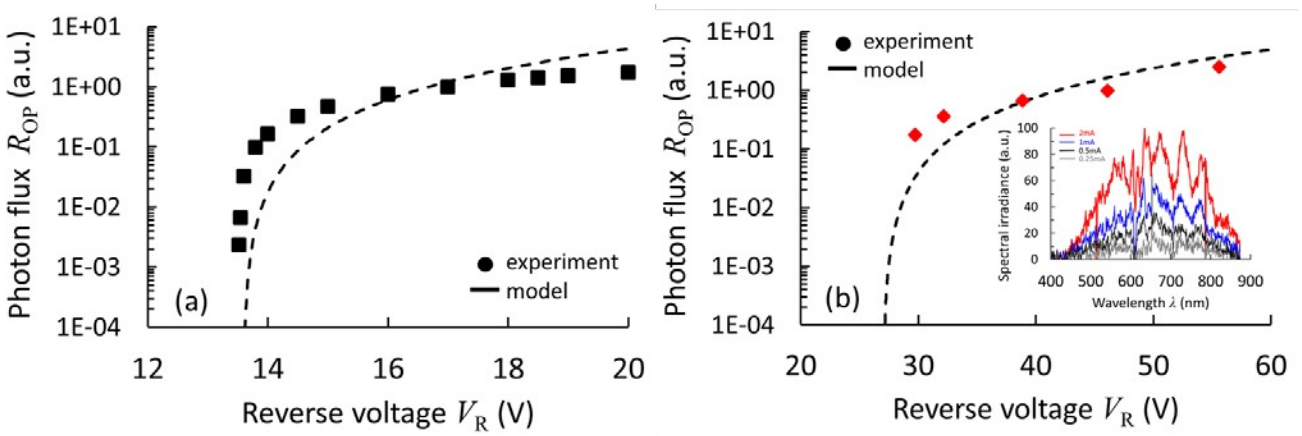

Figure 10 Measured (symbols) versus modeled (Eq. (13)) trend of the integrated photon emission flux R_{op} for (a) a vertical diode [41] and (b) an SJ diode (d=0.8µm). Inset: emission spectra for the SJ diode.

According to Eqs. (13)-(14) η_{RAD} has a linear dependence with the injector components J_{n0}, J_{p0}. Therefore it can be increased even more by adopting for instance an LED with a separate minority carrier injector as was reported earlier [3], [19], referred to as the CMOS n^+pp^+ LED. Interestingly, it was reported [42] that the external quantum efficiency of such CMOS n^+pp^+ LEDs also increases linearly with the injector current.

For yet better FOMs the injection-avalanche CMOS SJLED, *i.e.* a combination of a separate charge carrier injector and the SJLED, is proposed. Fig. 11 (a) shows an example in a bipolar transistor configuration. For a high injection current, hence efficiency, the base Gummel number should be small. A challenge however is to prevent nasty reliability issues caused by the positive feedback of the impact-ionization generated current in the bipolar transistor. This can be done by minimizing the current gain of the transistor as well. Other SJ configurations such as LDMOS or FinFET structures could also be employed. Another example could be to use an LDMOS structure in which RESURF is obtained via isolated electrodes, *i.e.* field-plate assisted RESURF [43], [21], see Fig. 11 (b). Also here the current gain of the (parasitic) bipolar transistor formed should be minimized, while there is sufficient carrier supply to the multiplication region. Finally, in advanced FD-SOI processes actual p-i-n diodes could be realized. Although in this case the buried oxide layer should be relatively thick compared to the multiplication length in the Si, which is not obvious on a commercial basis (hence standard CMOS).

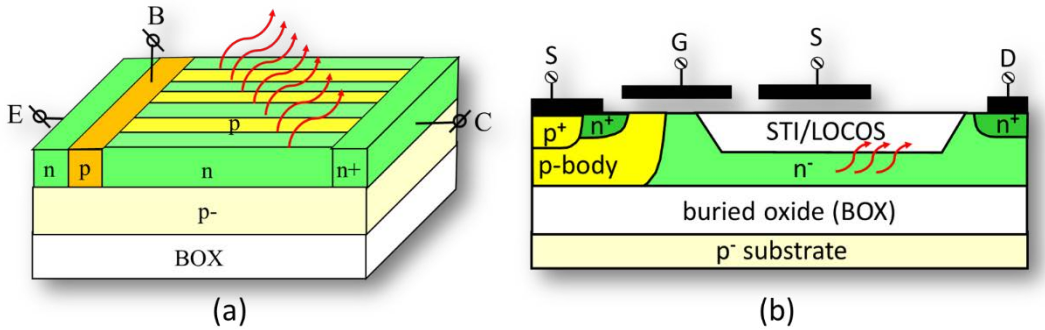

Figure 11 Examples of injection-avalanche RESURF CMOS devices: (a) Bird's eye view of a bipolar transistor with SJ collector region, (b) Schematic cross-section of an LDMOS realized in SOI-BCD processes making use of field-plate assisted RESURF [43], [21] via isolated electrodes (source, substrate), thereby obtaining a more uniform electric field distribution.

4. CONCLUSIONS

Closed form physics-based models for the key figures of merit, namely, avalanche current density, speed, radiative efficiency, and energy cost per photon of avalanche-mode light emitting diodes have been derived. Various optimized device structures have been evaluated. Good agreement of modeled trends is obtained with TCAD simulations and some measurements. The results show that in terms of design scalability, power, speed, optical efficiency and energy cost per photon, for the AMLED design a p-i-n or an optimized SJ diode is favorable to a conventional single-sided junction. In addition, as confirmed by reported data for conventional AMLEDs, the results indicate that for a yet higher efficiency the carrier supply should be increased. For this a combination of a separate minority carrier injector and RESURF LED is proposed, referred to as injection-avalanche CMOS RESURF LEDs. This work can serve as a guideline for device design and compact modeling of avalanche-mode LEDs, however, more experimental optical data (*e.g.*, absolute photon flux) are needed for a more accurate model validation and/or parameter extraction.

ACKNOWLEDGEMENTS

This work was partially funded by the Netherlands Organisation of Scientific Research (NWO) Domain Applied and Engineering Sciences, The Netherlands, under Project 12835. The authors would like to thank Prof.dr. Peter Steeneken and Prof.dr. Lis Nanver for providing the experimental support. Also, staff members of the Integrated Devices and Systems (IDS) and Integrated Circuit Design (ICD) groups are kindly acknowledged for their support.

APPENDIX

As discussed earlier [26], for having optimal RESURF the F_y expansion should be such that at breakdown (1) the depletion layer edge of each 1-D diode formed by a p- and n-pole should reach that of other 1-D diodes at its opposite side, and (2) the field perpendicular to the current flow direction of the SJ device (F_y, see Fig. 2) should not exceed the critical field at breakdown F_C of the 1-D diodes which are formed by the multiple pn poles.
For the perpendicular or *y*-field it can be derived that:

$$F_y(y) = F_{y,\mathrm{m}} - \frac{qN_\mathrm{D}}{\varepsilon_\mathrm{s}} \cdot y, \tag{A1}$$

with ε_s is the silicon permittivity.
At breakdown the field at the middle of the pole width $y=d$ equals zero, and therefore from Eq. (A1) it can be stated that

$$F_{y,\mathrm{m}} = \frac{qN_\mathrm{D}}{\varepsilon_\mathrm{s}} \cdot d \leq F_\mathrm{C} \approx 3 \cdot 10^5\ \mathrm{V/cm}, \tag{A2}$$

and hence,

$$N_\mathrm{D} \cdot d \leq F_\mathrm{C} \cdot \frac{\varepsilon_\mathrm{s}}{q} \approx 2 \cdot 10^{12}\ \mathrm{cm^{-2}}. \tag{A3}$$

Eq. (A3) indicates that for optimal RESURF there is a maximum limit for the product of the pole width *d* and doping concentration. This also implies that for p- and n-poles different doping concentrations (asymmetric superjunctions) can be used provided that the pole width is changed according to Eq. (A3).
Finally, in this discussion periodic boundary conditions are assumed: multiple p- and n-poles are infinitely repeated in the *y*-direction. However, obviously any device has finite dimensions and so the edge termination of the SJ device should be taken care of, otherwise premature edge breakdown could occur which is not desired. In our SJLEDs we designed the edge termination by adopting a half a pole width for the poles that are at the device periphery, and placed them next to the shallow-trench isolation (STI) regions.

REFERENCES

[1] Chynoweth, A.G. and McKay, K.G., "Photon emission from avalanche breakdown in silicon", Phys. Rev., 102(2), pp. 369- 376 (1956).

[2] Shewchun, J. and Wei, L.Y., "Mechanism for reverse-biased breakdown radiation in p-n junctions", Solid-State Electron., 8, pp. 485-493 (1965).

[3] Snyman, L.W., du Plessis, M., and Aharoni, H., "Injection-avalanche based n+pn silicon complementary metal–oxide–semiconductor light emitting device (450–750 nm) with 2-order-of-magnitude increase in light emission intensity", Jpn. J. Appl. Phys. 46(4B), pp. 2474-2480 (2007).

[4] van Drieënhuizen, B.P. and Wolffenbuttel, R.F., "Optocoupler based on the avalanche light emission in silicon", Sensors and Actuators A, 31(1), pp. 229-240 (1992).

[5] Chatterjee, A., Bhuva, B., and Schrimpf, R., "High-speed light modulation in avalanche breakdown mode for Si diodes", IEEE Electron Device Lett., 25(9), pp. 628-630 (2004).

[6] Snyman, L.W. *et al*., "Optical sources, integrated optical detectors, and optical waveguides in standard silicon CMOS integrated circuitry", Proc. SPIE, 3953, pp. 20-36 (2000).

[7] du Plessis, M., Aharoni, H., and Snyman, L.W., "Silicon LEDs fabricated in standard VLSI technology as components for all silicon monolithic integrated optoelectronic systems", IEEE J. Sel. Top. Quant. Electr., 8(6), pp. 1412-1419 (2002).

[8] Huang, B. *et al*., "CMOS monolithic optoelectronic integrated circuit for on-chip optical interconnection", Opt. Commun., 284, pp. 3924-3927 (2011).

[9] Khanmohammadi, A., Enne, R., Hofbauer, M., and Zimmermann, H., "Monolithically integrated optical random pulse generator in high voltage CMOS technology", ESSDERC proceedings, pp. 138-141 (2015).

[10] Xu, K., “Silicon light-emitting device in standard CMOS technology”, Proc. 8th Int. Photon. OptoElectron. Meetings (2015).

[11] Dutta, S., Hueting, R.J.E., Agarwal, V., and Annema, A.J., “An integrated optical link in 140 nm SOI technology”, CLEO conference (2016).

[12] Agarwal, V. *et al*., “Low power wide spectrum optical transmitter using avalanche mode LEDs in SOI CMOS technology”, Optics Express, 25(15), p. 16981 (2017).

[13] Snyman, L.W., du Plessis, M., and Bellotti, E., “Photonic transitions (1.4eV–2.8 eV) in silicon pþnpþ injection-avalanche CMOS LEDs as function of depletion layer profiling and defect engineering”, IEEE J. Quant. Elec., 46(6), pp. 906-919 (2010).

[14] Hueting, R.J.E. *et al.*, “An Improved Analytical Model for Carrier Multiplication Near Breakdown in Diodes”, IEEE Trans. Electron Devices, 64(1), pp. 264-270 (2017).

[15] Sze, S.M. and Ng, K.K., “Physics of Semiconductor Devices”, 3rd edition, John Wiley & Sons, Inc., USA (2007).

[16] Dutta, S. *et al*., “Opto-electronic modeling of light emission from avalanche-mode silicon p+n junctions”, J. Appl. Phys., 118, p. 114506 (2015).

[17] Dutta, S. *et al*., “Optical Power Efficiency Versus Breakdown Voltage of Avalanche-Mode Silicon LEDs in CMOS”, IEEE Electron Device Lett., 38(7), pp. 898-901 (2017).

[18] Dutta, S. *et al*.,”The Avalanche-Mode Superjunction LED”, IEEE Trans. Electron Devices, 64(4), pp. 1612-1618 (2017).

[19] Snyman, L.W. *et al.*, “Higher intensity SiAvLEDs in an RF bipolar process through carrier energy and carrier momentum engineering”, IEEE J. Quantum Electron., 51(7) (2015).

[20] Xu, K., “On the design and optimization of three-terminal light-emitting device in silicon CMOS technology”, IEEE J. Sel. Topics Quantum Electron., 20(4), (2014).

[21] Wessels, P. *et al*., “Advanced BCD technology for automotive, audio and power applications”, Solid-State Electron., 51(2), pp. 195–211 (2007).

[22] Kaneda, S. and Shirota, S., “New type of varactor diode consisting of multilayer p-n junctions”, Proc. IEDM, pp. 107-110 (1977).

[23] Appels, J. A. and Vaes, H. M. J., “High voltage thin layer devices (RESURF devices)”, Proc. IEDM, pp. 238–241 (1979).

[24] Coe, D. J., “High voltage semiconductor device”, U.S. Patent 4 754 310 A, Jun. 28 (1988).

[25] Tihanyi, J., “Power MOSFET”, U.S. Patent 5 438 215, Aug. 1 (1995).

[26] Fujihira, T., “Theory of semiconductor superjunction devices”, Jpn. J. Appl. Phys., 36(10), pp. 6254–6262 (1997).

[27] Udrea, F., Popescu, A., and Milne, W.I., “3D RESURF double-gate MOSFET: A revolutionary power device concept”, Electron. Lett., 34(8), pp. 808–809 (1998).

[28] Lorenz, L., Deboy, G., Knapp, A., and Marz, M., “COOLMOS—A new milestone in high voltage power MOS”, Proc. Int. Symp. Power Semiconductor Devices ICs (ISPSD), pp. 3–10 (1999).

[29] Ludikhuize, A. W., “A review of RESURF technology”, Proc. Int. Symp. Power Semiconductor Devices (ISPSD), pp. 11–18 (2000).

[30] Ferrara, A. *et al*., “Ideal RESURF Geometries”, IEEE Trans. Electron Devices, 62(10), pp. 3341-3347 (2015).

[31] Fulop, W., “Calculation of avalanche breakdown voltages of silicon p−n junctions”, Solid-State Electron., 10, pp. 39-43 (1967).

[32] Agarwal, V. *et al*., “Data Transmission Capabilities of Silicon Avalanche Mode Light-Emitting Diodes”, Accepted for IEEE Trans. Electr. Dev., 65 (2018).

[33] McCullagh, M.J. and Wisely, D.R., “155 Mbit/s optical wireless link using a bootstrapped silicon APD receiver,” Electr. Lett., 30(5), pp. 430-432 (1994).

[34] Marsh, G.W. and Kahn, J.M., “50-Mb/s Diffuse Infrared Free-Space Link Using On-Off Keying With Decision-Feedback Equalization”, IEEE Photonics Techn. Lett., 6(10), pp. 1268-1270 (1994).

[35] Schubert, E.F., “Light Emitting Diodes”, Cambridge University Press (2006).

[36] Sano, N. and Yoshii, A., “Impact-ionization theory consistent with a realistic band structure of silicon”, Phys. Rev. B, 45(8), pp. 4171–4180 (1992).

[37] Swoger, J. H. and Kovacic, S. J., “Enhanced luminescence due to impact ionization in photodiodes”, J. Appl. Phys., 74(4), pp. 2565–2571 (1993).

[38] Schlangenotto, H., Maeder, H., and Gerlach, W., “Temperature dependence of the radiative recombination coefficient in silicon”, Phys. Status Solidi A, 21, p. 357 (1974).

[39] Trupke, T. *et al*., “Temperature dependence of the radiative recombination coefficient of intrinsic crystalline silicon”, J. Appl. Phys., 94(8), pp. 4930-4937 (2003).

[40] Puliyankot, V., Piccolo, G., Hueting, R.J.E., and Schmitz, J., “Toward GHz Switching in SOI Light Emitting Diodes”, IEEE Trans. Electr. Dev., 65(10), pp. 4413-4420 (2018).

[41] Qi, L. *et al*., “UV-sensitive low dark-count PureB single-photon avalanche diode”, IEEE Trans. Electron Devices, 61(11), pp. 3768-3774 (2014).

[42] Snyman, L.W., Aharoni, H., and du Plessis, M., “A Dependency of Quantum Efficiency of Silicon CMOS n^+pp^+

LEDs on Current Density”, IEEE Photon. Techn. Lett., 17(10), pp. 2041-2043 (2005).

[43] Merchant, S., “Analytical model for the electric field distribution in SOI RESURF and TMBS structures”, IEEE Trans. Electr. Dev., 46(6), pp. 1264-1267 (1999).